FOI
SWEDISH DEFENCE
RESEARCH AGENCY

FOI-R--0139--SE
April 2001
ISSN 1650-1942

Methodology Report

Split-beam correlation processing

Elias Parastates
Mika Levonen
Bernt Nilsson
Per Söderberg

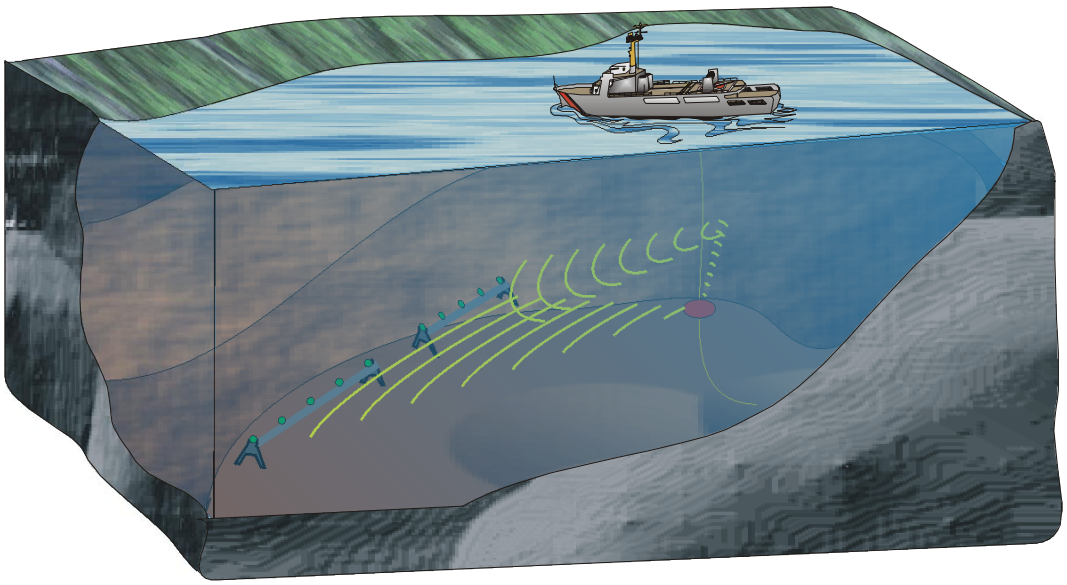

Division of Systems Technology
SE-172 90 STOCKHOLM

SWEDISH DEFENCE RESEARCH AGENCY
Division of Systems Technology
SE-172 90 STOCKHOLM
Sweden

FOI-R--0139--SE
April 2001
ISSN 1650-1942
Methodology report

Split-beam correlation processing

Elias Parastates
Mika Levonen
Bernt Nilsson
Per Söderberg

Issuing organization	Report number, ISRN	Report type
FOI - Swedish Defence Research Agency Division of Systems Technology SE-172 90 STOCKHOLM Sweden	FOI-R--0139--SE	Methodology Report
	Research area code **4. C4ISR**	
	Month year April 2001	**Project No.** E6031
	Customers code 1. Research for the Government	
	Sub area code 42 Surveillance Sensors	
Author/s (editor/s) Elias Parastates, Mika Levonen, Bernt Nilsson, Per Söderberg	**Project manager** Jörgen Pihl	
	Approved by	
	Scientifically and technically responsible Elias Parastates	

Report title

Split-beam correlation processing

Abstract

Split-beam correlation is a technique for passive bearing estimation of underwater sound sources. Split-beam correlation processing can be an attractive alternative in surveillance by means of towed arrays or when using several linear arrays installed at the sea bottom. The main advantage compared to classical beamforming, evident in high Signal to Noise Ratio (SNR) situations, is improved bearing resolution.

This work demonstrates the development of a computer code for split-beam processing. A future scope with the implementation of this method is to study its applicability in shallow waters. The horizontal arrays to be utilized should contain many wavelengths of the source signal components and still be populated by sensors separated by a moderate fraction of a half-wavelength. A rule of thumb is derived here for accessing the multipath interference that may occur in such environments.

Field measurements carried out in coastal shallow waters are analysed. Coherence measurements indicate that for frequencies below 250 Hz the experimental site most often supports coherence lengths of the order of 200 m. The expected trend of coherence improvement with decreasing frequency is not evident. For the higher frequencies this behavior could be explained by changes in the speed of sound and sea surface roughness, affecting the multipath propagation within the shallow water channel in a different way during each measurement. With a few exceptions, coherence did improve with decreased hydrophone separation distances.

Split-beam processing is carried out using signals from an approximately horizontal linear array, with the same aperture as the experimentally deduced coherence lengths. The array is sparsely populated with hydrophones. The sensor spacing is up to fifteen times larger than what should be appropriate for the source signal bandwidth utilized. Grating lobes are introduced as a consequence, and the array gain becomes severely degraded. The coastal environment hosting the array, causes source signal reflection from shore, further increasing the destructive impact of the grating lobe presence. The beam power versus bearing plots did indicate the position of the sound source but they did also show a number of false bearing indications most likely due to the grating lobe issue. No statement about the ultimate performance of the split-beam correlation technique can therefore be made on the basis of the processed data.

Key words

Beamformning, product arrays, underwater acoustics, signal processing, coherence

Further bibliografic information	Language English
ISSN 1650-1942	**Pages** 17 p
	Price Acc. to pricelist **Security classification** Unclassified

Utgivare	Rapportnummer, ISRN	Klassificering
Totalförsvarets Forskningsinstitut - FOI Avdelningen för Systemteknik 172 90 STOCKHOLM	FOI-R--0139--SE	Metodrapport
	Forskningsområde 4. Spaning och ledning	
	Månad år April 2001	**Projektnummer** E6031
	Verksamhetsgren 1. Forskning för regeringens behov	
	Delområde 42 Spaningssensorer	

Författare (redaktör)	Projektledare
Elias Parastates, Mika Levonen, Bernt Nilsson, Per Söderberg	Jörgen Pihl
	Godkänd av
	Tekniskt och/eller vetenskapligt ansvarig Elias Parastates

Rapportens titel

Split-beam korrelationsprocessering

Sammanfattning

Split-beam korrelation är en teknik för passiv bäringsbestämning till en undervattensljudkälla. Tekniken kan vara ett attraktivt spaningsalternativ för bogserade antenner eller när flera linjära antenner installerats på bottnen. Det främsta fördelen jämfört med klassisk lobformning är den förbättrade upplösningen i bäring speciellt vid höga signal/brus-förhållanden.

Föreliggande rapport behandlar tillämpningar för split-beam tekniken. Syftet är att i framtiden kunna studera metodens tillämpbarhet inom grunda vattenområden. En sådan studie kräver en horisontell antenn med en apertur som innehåller många våglängder av den högsta signalfrekvensen och där de enskilda hydrofonerna har ett inbördes avstånd av minst en halv våglängd.

Data från fältförsök i kustnära grunda vatten har analyserats och presenteras i denna rapport. Koherens-mätningarna indikerar att miljön i detta fall gynnar koherens-längder i storleksordningen 200 m för frekvenser under 250 Hz. Den förmodade förbättrade koherensen med sjunkande frekvens är inte uppenbar. I fallet med högre frekvenser kan denna iakttagelse förklaras med förändringar av ljudhastigheten inom vattenpelaren och av vågrörelser i vattenytan som inverkar på strålgången inom grunda vattenområden. Med några undantag ökade koherensen med minskat avstånd mellan hydrofonerna.

Split-beam analysen är utförd på data från en i stort sett horisontell antenn med samma apertur som den experimentellt härledda koherenslängden. Antennens element satt tämligen glest. Avståndet mellan hydrofonerna var upp till femton gånger längre än vad som skulle ha varit lämpligt för ljudkällans bandbredd. Som en konsekvens härav bildas störande sidolober. I synnerhet bidrar den kustnära miljön störande med bland annat ljudreflexer från omgivningen. Lobeffekten som funktion av bäringen visar läget för ljudkällan men också ett antal falska riktningar troligen beroende av de kraftiga sidoloberna. Inget slutgiltigt resultat kan därför presenteras genom split-beam korrelationen utifrån de data som har analyserats.

Nyckelord

Bäringsbestämning, produktantenner, hydroakustik, signalbehandling, koherens

Övriga bibliografiska uppgifter	Språk Engelska
ISSN 1650-1942	**Antal sidor** 17
Distribution enligt missiv	**Pris** Enligt prislista **Sekretess** Öppen

Contents

1. Introduction

A split-beam processing technique [1, page 127] in sonar array applications addresses the estimation of bearings for underwater sound sources by means of a passive linear array. The receiver array is assumed to consist of two subarrays placed towards the ends of its aperture. As a first step, beams from each sub array are computed by means of classical beamforming. As a second step, assuming the source signals to be of broadband nature, beams from each sub array, formed by steering in the same direction, are cross-correlated in order to obtain time-lags for bearing estimation.

Split-beam processing could be an attractive alternative in passive surveillance by means of towed arrays or when using several linear arrays installed at the sea bottom, pair wise located along the same base line. The main advantage compared to classical beamforming, evident in high Signal to Noise Ratio (SNR) situations, is improved bearing resolution. [2, 3]

Stergiopoulos and Ashley [4] observed that the split-beam performance improvement over the conventional full aperture beamformer could be practically insignificant due to the split-beamformer´s poor ability to detect low SNR broadband signals. They also pointed out that despite these performance problems the split-beam processing concept attracts sonar system designers because it is easier from a computing architecture point of view.

This work demonstrates the implementation of a split-beam correlation algorithm by simulations and experimental data analyses. The basic assumptions made are that noise processes sampled by different hydrophones are stationary Gaussian and mutually statistically independent. Furthermore the source signal is supposed to be generated from a sufficiently distant source so that its wave front may be regarded as planar over the array aperture, i.e. the plane wave approximation applies.

The present implementation is aimed for a future study of the applicability of the split-beam technique for shallow water experimental data. The data are to be collected by horizontal arrays containing many wavelengths of the source signal components and still being populated by hydrophones separated by a moderate fraction of a half-wavelength.

The data analysed herein were collected in Djupviken, a bay of the Baltic Sea, using an array of few hydrophones with considerably larger spacing than what is appropriate. The reported results may therefore not reflect the ultimate performance of the processing technique utilized. The particular choice of experimental site, array configuration as well as the choice of the rather weak excitation source was imposed by the available equipment.

Array processing of signals from non-moving sources using a moored array often requires the coherence lengths to be of the same magnitude as the array aperture. A previous work by Westerlin [5] indicates that this requirement is fulfilled regarding apertures of same magnitude as in the Djupviken experiment. Westerlins conclusions are made when processing data from other experimental sites, during different weather conditions and sea states and may not necessarily be valid regarding Djupviken. A number of coherence measurements did therefore precede the split-beam processing experiment.

This work is arranged as follows. In section 2 the coherence estimation is reviewed and the split-beamforming processing is described and demonstrated by a numerical simulation. Experimental results regarding coherency lengths and bearing estimation are reported in section 3. Some additional remarks are made in section 4. Section 5 gives a concluding summary.

2. Method

2.1 Split-beam processing

Assume an oceanic medium with a linear horizontal array of receivers sampling a stationary random field composed by plane wave contributions from distant sources and spatially as well as temporally uncorrelated environmental noise. Assume the receivers to be arranged in two subapertures of N receivers each. Designate the horizontal receiver coordinates by $\mathbf{r}_{l,n} \in R^{2\times1}$, l=1, 2, n=1,...N where l=1 and l=2 correspond to the left and right subaperture respectively. The array configuration is shown in Figure 1.

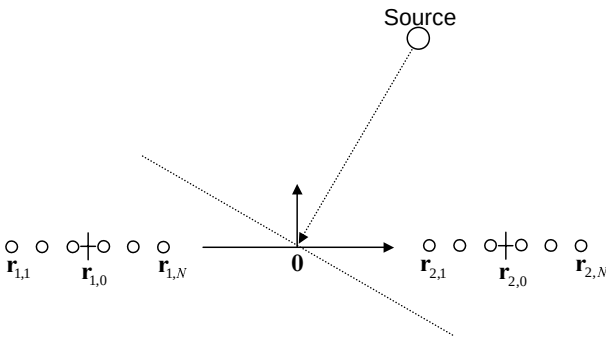

Figure 1. *The array geometry plus a plane wave contribution from a distant source. The phase centres of the left and right sub aperture are designated by* $\mathbf{r}_{1,0}$ *and* $\mathbf{r}_{2,0}$ *respectively.*

Denote the correlation of signals from sensors at coordinates $\mathbf{r}_{k,m}$ and $\mathbf{r}_{l,n}$ as a function of time-lag τ, by $\rho(\mathbf{r}_{k,m},\mathbf{r}_{l,n},\tau)$. Introduce the cross spectral density matrices $\mathbf{C}_{k,l}(\omega)\in C^{N\times N}$, k=1, 2, l=1, 2, where ω designates the radial frequency, with cross spectral densities

$$\mathbf{C}_{k,l}(\omega,m,n)=\int_{-\infty}^{\infty}\rho(\mathbf{r}_{k,m},\mathbf{r}_{l,n},\tau)e^{-i\,\omega\,\tau}d\tau \qquad (1)$$

as elements. When the sensor positions coincide $\mathbf{C}_{k,k}(\omega,m,m)$ becomes the Power Density Function (PDF) corresponding to the auto correlation function $\rho(\mathbf{r}_{k,m},\mathbf{r}_{k,m},\tau)$ with signal power $\rho(\mathbf{r}_{k,m},\mathbf{r}_{k,m},0)$. The coherence function

$$\gamma^2(\omega,\mathbf{r}_{k,m},\mathbf{r}_{l,n})=\frac{\left|\mathbf{C}_{k,l}(\omega,m,n)\right|^2}{\mathbf{C}_{k,k}(\omega,m,m)\mathbf{C}_{l,l}(\omega,n,n)} \qquad (2)$$

may be regarded as a cross spectral density normalized to the region $\gamma^2(\omega,\mathbf{r}_{k,m},\mathbf{r}_{l,n})\le1$. Introduce the steering vector

$$\mathbf{a}_l(\omega,\theta)= \qquad (3)$$
$$\left(e^{-i\omega\mathbf{n}^{\mathrm{T}}(\theta)(\mathbf{r}_{l,1}-\mathbf{r}_{l,0})/c}\quad\cdots\quad e^{-i\omega\,\mathbf{n}^{\mathrm{T}}(\theta)(\mathbf{r}_{l,N}-\mathbf{r}_{l,0})}\right)^{\mathrm{T}}\in C^{N\times1}$$

where $\mathbf{n}(\theta)\in R^{2\times1}$ is the unit vector normal to a wave front impinging to the array from bearing θ and $\mathbf{r}_{l,0}$ is the phase center coordinate of the aperture. The velocity of sound is denoted by c. The elements of the steering vector are plane wave approximations of the free space Greens function. Introduce the expression

$$d_{k,l}(\omega,\theta)=\mathbf{a}_k^{\mathrm{H}}(\omega,\theta)\mathbf{C}_{k,l}(\omega)\mathbf{a}_l(\omega,\theta) \qquad (4)$$

For a fixed bearing angle and k=l, the quadratic detector $d_{l,l}(\omega,\theta)$ equals to the beam PDF of aperture l. The beam power is defined as the integral of the beam PDF over the frequency region of interest. If the wavefield is homogenous, i.e. $\rho(\mathbf{r}_{k,m},\mathbf{r}_{l,n},\tau)$ $=\rho\left(\left\|\mathbf{r}_{k,m}-\mathbf{r}_{l,n}\right\|_2,\tau\right)$ then it is possible to define the split-beam correlation function

$$s(\alpha,\theta)=\int_{-\infty}^{\infty}d_{1,2}(\omega,\theta)e^{-i\,\omega\,\alpha}d\omega \qquad (5)$$

where $\alpha=\mathbf{n}^{\mathrm{T}}(\theta)(\mathbf{r}_{1,0}-\mathbf{r}_{2,0})/c$. For a fixed bearing, the value $\alpha=\alpha_s$ that maximizes (5) can be interpreted as the split-beam processing bearing estimate

$$\theta_s=\cos^{-1}\left(c\,\alpha_s/\left\|\mathbf{r}_{1,0}-\mathbf{r}_{2,0}\right\|_2\right). \qquad (6)$$

2.2 A numerical simulation

A numerical simulation here illustrates the previously described processing scheme. Two linear subapertures record a sound source in complete absence of noise. There are 6 sensors in each subaperture located at the distances -26 m, -9 m, 1 m, 11 m, 24 m, 26 m and –26 m, -24 m, -10 m, 2 m, 13 m, 26 m relative to the left and right subaperture phase center respectively. The phase center separation $\left\|\mathbf{r}_{1,0}-\mathbf{r}_{2,0}\right\|_2$ =150 m. A second order Butterworth-filter with pass band region between frequencies 60 Hz and 200 Hz is applied to the array signal. The PDF of the source signal before and after filtering is shown in Figure 2.

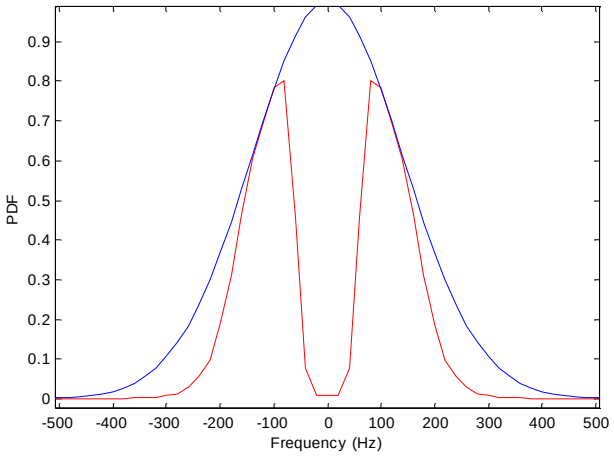

Figure 2. *The PDF of the source signal before (blue) and after filtering (red).*

Figure 3 shows one period of the source signal propagating towards the array.

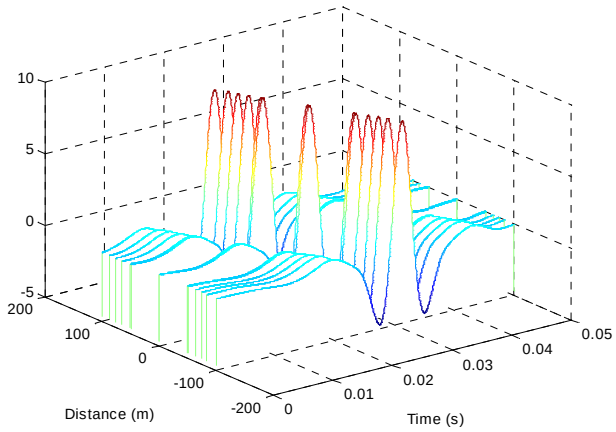

Figure 3. *One period of the source signal propagating towards the array.*

The beam PDF as a function of steering angle for each subaperture is shown in Figure 4. These kinds of plots are usually referred to as FRequency Azimuth (FRAZ) plots. For a fixed frequency the beam PDF regarded as a function of steering angle contains, apart from the maximum located at the source bearing, a number of peaks related to the side lobes. The side lobe locations vary with frequency while the maxima stack up at the same bearing. Apart from localization, FRAZ plots may be used for classification by spotting signatures in the beam PDF.

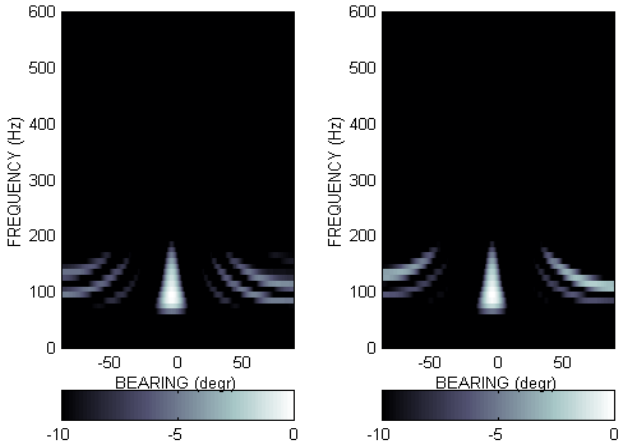

Figure 4. *FRAZ plots for left and right subapertures.*

Figure 5 shows the beam power as a function of steering angle and time for each subaperture. The time axis indicates the location in time of the data records – here source signal periods – utilized for a beam PDF computation. The beam power is essentially computed by incoherent integration of the beam PDF, seen in previous figure, over the frequency axis. The integration averages out peaks related to side lobes. A plot of this kind, usually referred to as Bearing Time Records (BTR) may be used to continuously track a moving source. Here, since the source is fixed, each plot shows a single straight line at - 5° – the true source bearing.

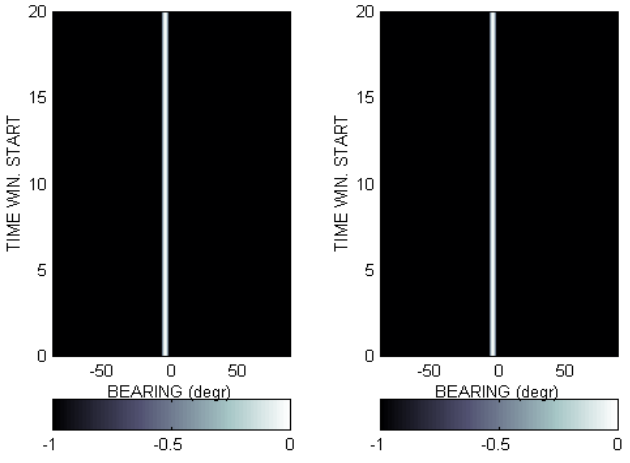

Figure 5. *BTR plots for left and right subaperture.*

The beam power averaged over the number of data records as a function of steering angle is shown in Figure 6. This kind of averaging is applicable in cases where the source is fixed during the incoherent integration time.

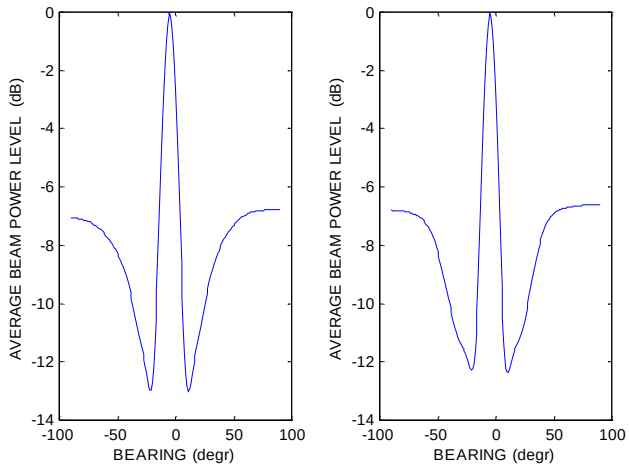

Figure 6. *Average beam power for the left and right subapertures as a function of steering angle. The number of data records was 20.*

Finally Figure 7 shows the correlation between pairs of left and right aperture beams, usually referred to as the split-beam correlation, as a function of time lag and steering angle, incoherently averaged over the number of data records.

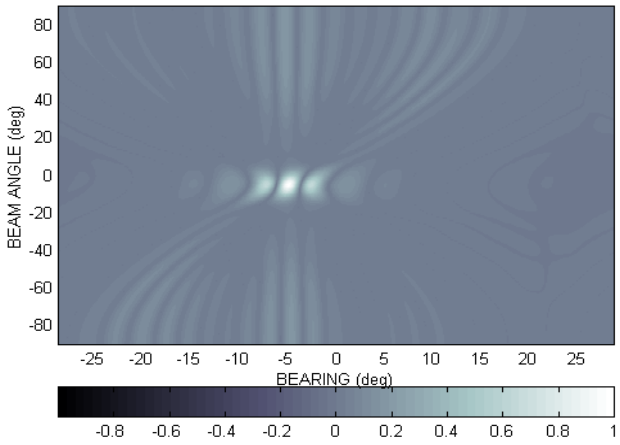

Figure 7. *The split-beam correlation, incoherently averaged over the number of data records. Beam angle (y-axis) indicates the angle of beam pairs being correlated. Bearing angle (x-axis) is constituted by the time-lag transformed to the angle domain.*

The main lobe in the plot indicates the true source bearing. Beam angle (y-axis) indicates the angle of beam pairs being correlated. Hence a slice along a fixed beam angle yields the correlation function of the time domain representation of the beams. Bearing angle (x-axis) is constituted by the time lag transformed to the angle domain. The two lesser peaks in the plot are due to the spectral shape of the source signal. One way to further increase the bearing resolution is to normalize each frequency component within the pass band with its amplitude, transforming the source spectrum to a boxcar shape [4]. A disadvantage with the latter approach could be that all frequency components are weighted equally, which in low signal to noise ratio (per frequency bin) situations results in an amplification of the noise component.

3. Experimental results

3.1 Environment and experimental configuration

The seafloor at the test site consists of soft postglacial clay and mud, so called gyttja-clay with an organic content of ~3%. This is a rather inhomogeneous layer but with a persistent thickness of around 1.5 m. There are small variations of the distribution of the very uppermost softest layer, particles almost in suspension, throughout the site. In the most shallow parts, at water depth less than around 10 m, the top soft deposit seems to be slightly thinner compared to in deeper water. Most likely this is a result of the ordinary eroding swell of the shallower parts. The eroded particles are transported and deposited on deeper water. A map of the site including the hydrophone array and sound source positions is shown in Figure 8.

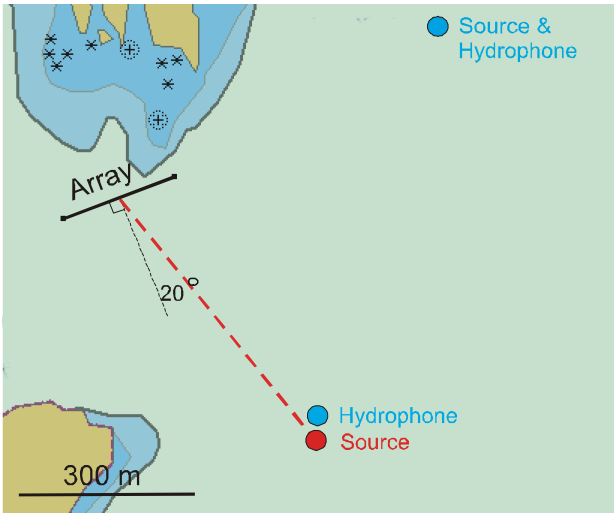

Figure 8. *Experimental configuration. Blue dots correspond to the coherence measurements. Red line indicates the source bearing in the split-beam experiment.*

In the vicinity of the most shallow part of the array, the bottom consist of till with minor boulders and pebbles. The seabed surface is smoothly undulating at the site and without any vegetation below a few meters depth. The maximum depth in the area is around 40 m.

The bases for the receiving array were five tripods lined up in water depth from 18 to 6 meters. Each tripod was equipped with two hydrophones at a height of 3 m over the bottom and with an individual spacing of 2 m. The tripods were spaced 50 m apart. Between the two outermost pairs of tripods three extra hydrophones were arranged with approximately equal spacing. The full configuration is shown in Figure 9.

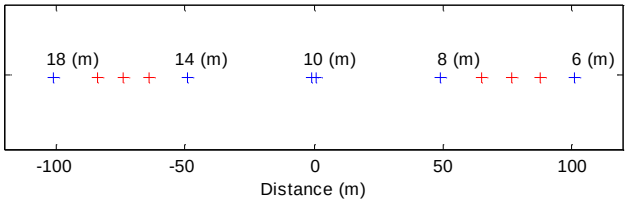

Figure 9. *The configuration of the array used in the Djupviken experiment. Blue crosses indicate sensors permanently fixed on tripods, 3 m over the bottom. The water depth is shown above each blue cross. Red crosses indicate additional sensors attached on a wire stretched between the tripods.*

The sound profile registered in connection to the measurements, reported herein, is shown in Figure 10.

During the days of the fieldwork the water temperature varied between around 12 centigrades at the surface and decreased with depth to reach 2 centigrades near the bottom at 40 m. The sound velocity at the surface varied between 1458 to 1462 m/s, decreasing to 1422– 1428 m/s at the bottom. The velocity is quite constant the uppermost 8 m whereafter it decreased down to 25 m with a more rapid decrease below that depth.

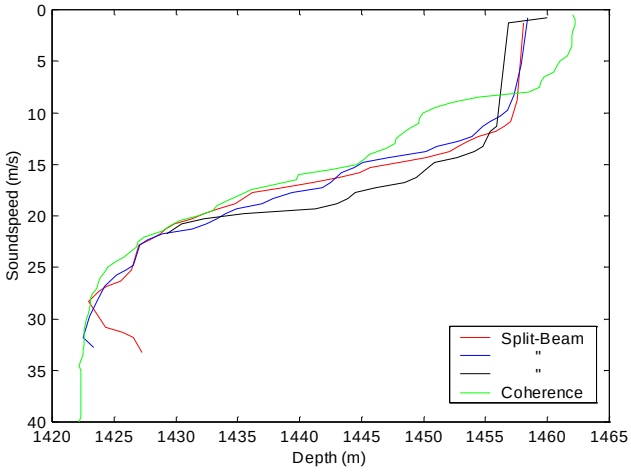

Figure 10. *The sound speed profiles registered in connection to the measurements. The registrations during the split-beam measurement were made with 5 hour intervals.*

3.2 Coherence

Measurements for coherence calculations were carried out using the array configuration shown in figure 9 (the blue crosses), with an addition of two extra hydrophones to obtain larger apertures.

One of the extra hydrophones was placed at an experiment vessel by the source.The other one on a second experiment vessel, see figure 8. The excitation source used was an omni-directional transmitter. Constant Wavelength (CW) signals were transmitted at the following frequencies, 63, 125, 250, 500, 1000, 2000, 4000, 6300, and 8000 Hz.

In order to correctly interpret the results of the coherence estimation, one needs to understand the properties of the received signals. First, for data quality monitoring, Fourier transforms of windowed sensor signals were calculated and plotted as functions of the time window location. Figures 11 and 12**,** the latter being a zoom of the low frequency region, exemplifies a case when the transmitted frequency was 4kHz.

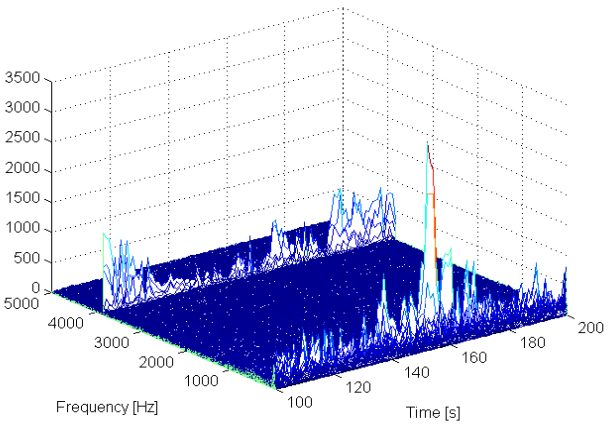

Figure 11. *Fourier Transform of a windowed signal, received by hydrophone 1, as a function of time window location. The time and frequency intervals were 100 – 200 s and 0 - 5 kHz respectively.*

Strong low frequency components appear in the spectra, especially at 50 Hz – the Swedish power line frequency.

The next observation from these time-frequency plots is that the levels vary with time. One contributing factor could be multipath propagation where travel times along individual paths vary with time. Consider for instance a case where a sensor samples signal contributions propagating along the direct and the surface reflected paths. Travel time pertaining to the surface reflection path will thereby be affected by wave rollers, which will result in a time dependent multipath interference at the sensor position. This effect also constitutes a deviation from the stationary field assumption, made in coherence estimations.

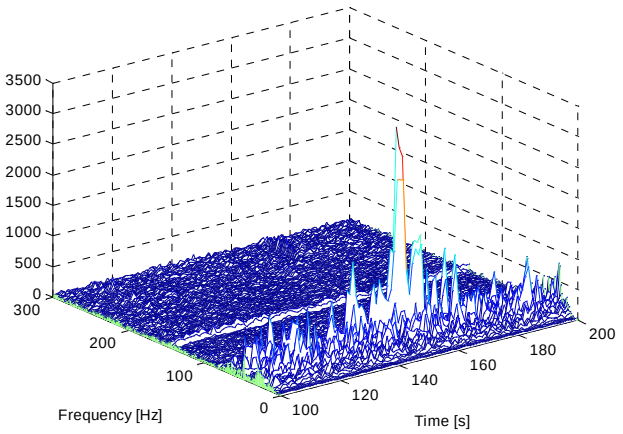

Figure 12. *Fourier Transform of a windowed signal, received by hydrophone 1, as a function of time window location. The time and frequency intervals were 100 – 200 s and 0 – 300 Hz respectively. This is a zoom of the spectrum in figure11.*

Furthermore the SNR (Signal to Noise Ratio) was calculated. The SNR levels were found to be about 40 dB at best. The levels varied least in the vicinity of the transmitter and most at the most distant hydrophone. The SNR decrease due to transmission loss is less than for the case of cylindrical propagation.

A few general issues about coherence and their compliance to our own observations follow below.

Experience has shown that coherence varies with the following parameters [6, page 193]:

- Separation of the receivers: Improves when the distance between the receivers decreases.
- Frequency: Improves with decreasing frequency.
- Bandwidth: Improves with decreasing bandwidth.
- Integration time: Improves with decreasing integration time, however the integration time needs to be long enough to obtain consistent estimates of coherence.
- Multipath structure: The coherence is high when there is a single dominant path, and multipaths are effectively absent.

Here, the issue of separation between the receivers, will involve the water sound speed profile at our measurement site. In Figure 10 the profile during the coherence measurements (green line), yields a strong downward bend of the propagation traces (see also section 4). It was noted that the hydrophones at a depth below the knee in the water sound speed profile have lower coherence values, than the ones above the knee. To make such a comparison, the coherence estimate was calculated using hydrophone 1 (leftmost in figure 9) as a reference; thereafter the coherence estimate was recalculated using hydrophone number six as a reference. This set up provides two hydrophones (1 and 2) below the knee and two hydrophones (5 & 6) above the knee. This leads to the obvious conclusion that spatial homogeneity does not hold completely for wavefields in range dependent media. Moreover the conclusion of lower values for the coherence with increasing distance does not hold completely.

By looking at Figures 13 and 14 it is not obvious that the coherence values in general decrease with increasing frequency. For the higher frequencies this behavior could be explained by changes in the speed of sound and wind (i.e. sea surface roughness), affecting the multipath propagation within the shallow water channel in a different way during each measurement.

The influence of bandwidth on coherence was investigated using different window lengths, 4 s, 1 s, and 0.25 s. Using windows longer than 4 s renders the averaging too short, while windows shorter than 0.25 s provide a poor frequency resolution. However, the coherence values are better for the longer window (smaller bandwidth).

The question of integration time, or rather number of averaged windows of the signal, was investigated by trying as few as 20 windows, compared to as many as 140 windows. The values were indeed higher for the lower number of averages. But it should be noted that the variance and bias of the coherence estimate is dependent on the number of averages, they go down as the number of averages increase, [7].

There are two frequencies in [5] that can be compared with the measurements mentioned above, 125 Hz and 6300 Hz, at a distance of 500 m. However, the integration time differs for the analysis bandwidth. In [5] the number of averages are 27 and 29 respectively, with coherence values equal to 1.00 and 0.67. The values

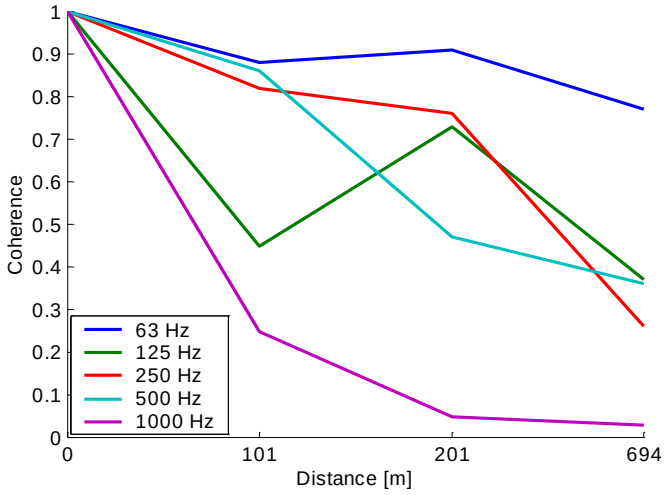

Figure 13. *Estimated coherence using hydrophone 1 as reference, for frequencies 63, 125, 250, 500, and 1000 Hz.*

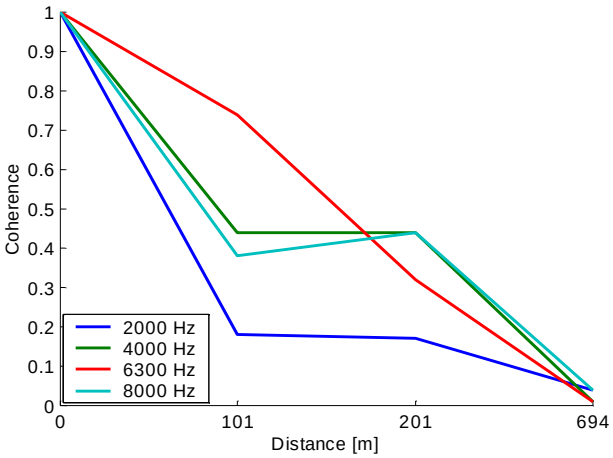

Figure 14. *Estimated coherence using hydrophone 1 as reference, for frequencies 2000, 4000, 6300, and 8000 Hz.*

obtained in this report are considerably less, 0.27 and 0.01, averaged over 140 spectras, at a distance of 694 m. Yet another difference between the two measurements should be noted, the water depth was between 25 m and 45 m in [5] compared to 8 m at the hydrophone at the most shallow point and about 40 m at the transmitter position.

3.3 Split-beam processing

Measurements for split-beam processing were carried out using the array configuration shown in figure 9. The excitation source, being an omni directional transmitter, was moored at several positions. At each position pink noise with different bandwidths and a spectrum roll off of 12 dB per octave, were transmitted. The registrations made by the additional hydrophones, marked with red crosses in figure 9, were distorted by power line interference frequently overflowing the analog to digital converters of the data acquisition system. Another factor for overflow was crackling sounds induced by mechanical vibrations of loosely suspended hydrophones due to wave rollers. Aural and visual quality monitoring of registered signals reduced the number of data sets. Several data sets were useless due to shipping noise. The data sets *Beam11005* and *Beam11006* analysed herein, Table 1, although still being partially distorted, are among the ones offering the best overall quality. The source was driven to a higher sound power level in the latter data set. The transmitted signal was pink noise in the region below 200 Hz. The source bearing relative to the array baseline normal was ~ –20°. Signals from additional hydrophones in both data sets have strong spectral components in the region of 30-50 Hz, probably due to power line interference. Tripod-hydrophones provided high quality registrations during 20 s (*Beam11005*) and 60 s (*Beam11006*). The parameter settings used in the split-beam processing of these data sets are shown in Table 1.

Figures 15, 16, and 17 show the FRAZ plots for datasets *Beam11005* and *Beam11006* respectively. In the processing leading to the first two figures the additional hydrophones were excluded in order to eliminate distortion due to power line interference. This was done at a cost of a reduced directivity index and introduction of grating lobes. The array gain along bearings corresponding to grating lobes, equals the gain along the steering angle corresponding to the main lobe. The occurrence of the grating lobes degrades the ability of the array to unambiguously measure bearings and discriminate presence of multiple targets or reflections from shore. Notice that spectral components above 100 Hz are almost absent in the FRAZ plot for *Beam11005*. In Figure 17 all hydrophones where used but the high pass frequency was increased in an attempt to reduce the power line interference. In this figure the beam corresponding to approximately 0° bearing contains strong spectral components not present in the other two plots. This effect indicates a strongly coherent noise component present in the additional sensors. Having in mind that individual bin beam patterns should stack up at the source bearing, it is difficult to distinguish any reliable estimate of the source bearing among all grating lobe contributions in those three FRAZ plots.

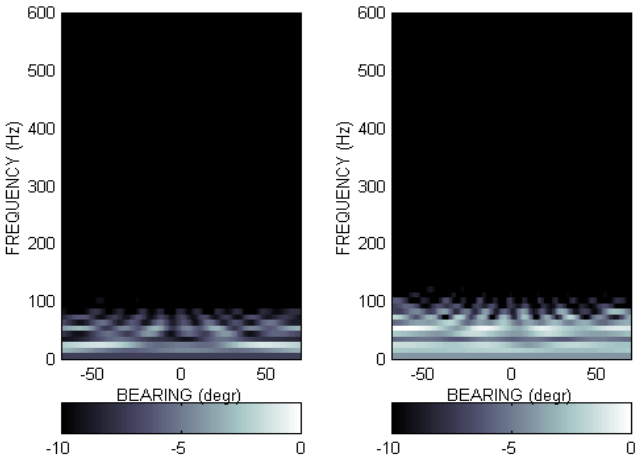

Figure 15. *FRAZ plots for data set Beam11005 using the tripod hydrophones.*

Table 1 The parameter settings used in processing of data sets in order to obtain the reported results. The source bearing relative to the array baseline normal was ~ –20°.

Data set	Analysis interval (s)	Nr. of windows	Record length (s)	Passband reg. (Hz)	Hydrophones
Beam11005	20	21	0.05	10-200	Tripod-phones
Beam11006	60	31	0.05	10-200	Tripod-phones
Beam11006	60	31	0.05	80-200	All

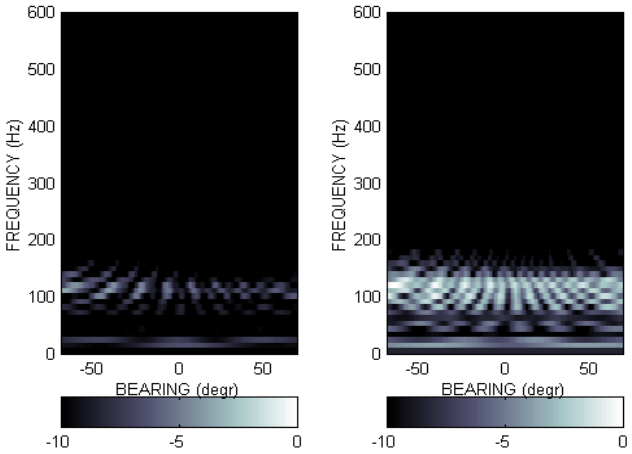

Figure 16. *FRAZ plots for data set Beam11006 using the tripod hydrophones.*

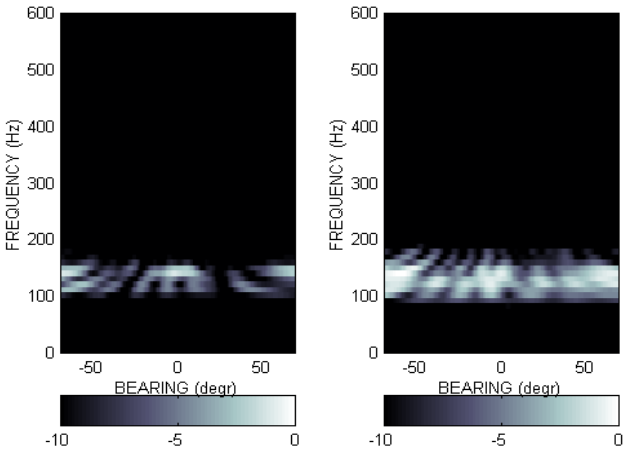

Figure 17. *FRAZ plots for data set Beam11006 using all hydrophones.*

Figures 18, 19 and 20 show the beam power averaged over the number of snapshots as a function of steering angle. Although the location of grating lobes varies with frequency and is averaged down for broadband signal surveillance the limited bandwidth of the source signal, being less than 200 Hz, limits this advantageous effect considerably. It is however possible to identify peaks located at the source bearing; lines in the figures mark those peaks. The remaining peaks could be due to reflections from shore; that issue is addressed further in the next section. Figure 20 has strong peaks at a bearing region around 0°, which is consistent with what is seen in the corresponding FRAZ plot. These peaks seem to be connected with the use of the additional hydrophones. One possible explanation for their presence could be cross talk between cables connecting the sensors with the data acquisition system, with the strongest sensor signal dominating. Another reason could be coherent noise induced by receiver electronics. In both cases beam power due to distortion would be superposed onto beam power due to sound. By inspection of the three figures it appears that the beam power at the source bearing is at least 3 dB less for the left sub aperture. This effect could be introduced by sound intensity variations due to the sound speed profile, see also next section.

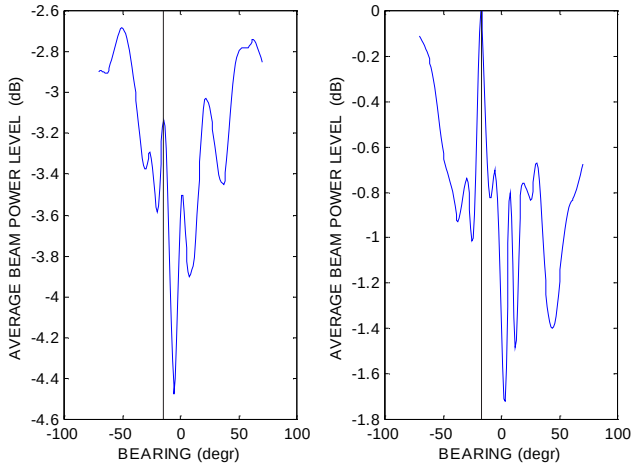

Figue 18. *Average beam power as a function of steering angle for data set Beam11005. Only the tripod hydrophones were used.*

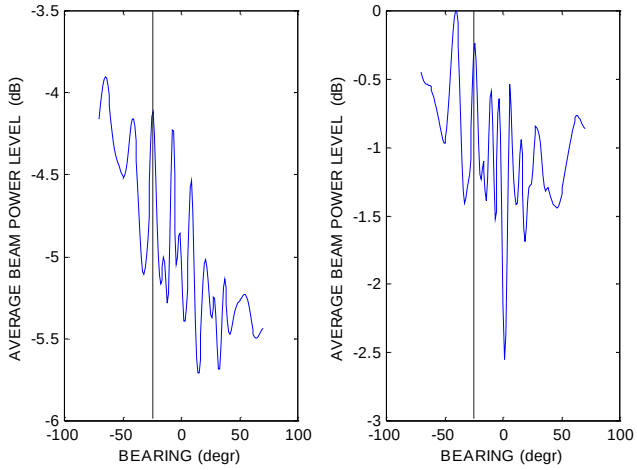

Figure 19. *Average beam power as a function of steering angle for data set Beam11006. Only the tripod hydrophones were used.*

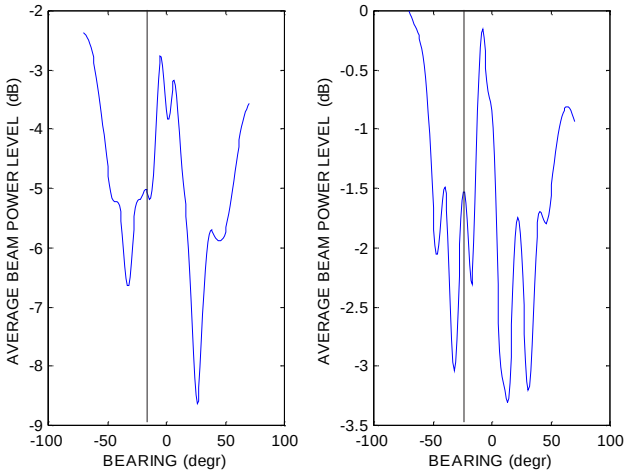

Figure 20. *Average beam power as a function of steering angle for data set Beam11006 when using all hydrophones.*

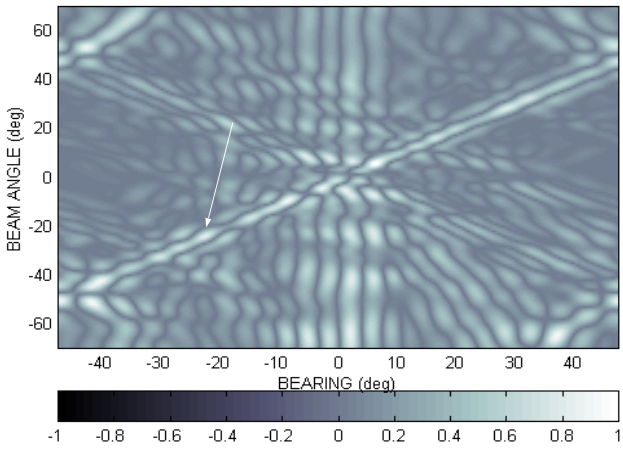

Figure 21. *Split-beam correlation plot for data set Beam11006 when using the tripod hydrophones. The source bearing is marked by an arrow.*

The low signal bandwidth in *Beam1105*, see Figure 15 degraded the performance of the split-beam former. The strong spectral contributions present at the bearing region around 0°, when processing all sensor signals of data set *Beam1106*, generated a dominating peak at same bearing in the split beam correlation plot. Figure 21 shows the split-beam correlation plot for the latter data set when only using the tripod hydrophones. Among a number of strong ambiguous peaks an arrow marks the true bearing estimate.

4. Additional remarks

The first issue considered is the complication occurring in the presence of multipath propagation. The aim is to get a rough understanding for the influence of multipath propagation by simple calculations. Consider the geometry pictured in Figure 22.

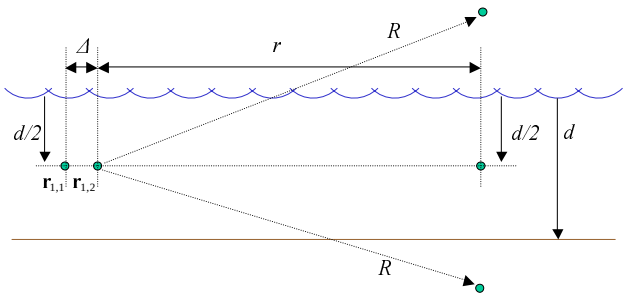

Figure 22. *Geometry of the multipath situation studied.*

Several assumptions are made. First, the two receiver positions, designated by $\mathbf{r}_{1,1}$ and $\mathbf{r}_{1,2}$, and the source are located in the middle of the water column with constant depth d and along the same base line. Second, the receiver separation distance $\|\mathbf{r}_{1,1} - \mathbf{r}_{1,2}\| = \Delta$ and the water depth d are small compared to the distance r between the source and the receivers. Finally a pressure release sea surface and a completely impenetrable bottom bound the water column. Let τ_l, l=1, 2 denote the difference in traveltime along a path with one boundary reflexion and the direct path; the subindex l indicates the receiver position. From previous assumptions, the figure geometry and a little algebra follows that

$$\tau_l \approx d^2/2rc = \tau_s,\ l = 1,2\ . \qquad (7)$$

Taking into account the surface reflexes only, the cross correlation of the received signals will be

$$\rho(\mathbf{r}_{1,1},\mathbf{r}_{1,2},\tau) = \rho_s(\tau-\theta)-\rho_s(\tau-\tau_s)-\rho_s(\tau+\tau_s-\theta)+\rho_s(\tau) \qquad (8)$$

where $\theta=\Delta/c$ and $\rho_s(\tau)$ is the autocorrelation function of the source signal. In the absence of multipath, the Right Hand Side (RHS) of (8) would contain only the first term. Since beamforming aims to estimate θ (or more generally, the time-delay between array elements), it is evident that multipath propagation poses a serious complication. From (7) follows that τ_s tends to zero as the source range r tends to infinity. As a consequence, the terms in the RHS of (8) cancel out. The approximate formula below will give an understanding for when this may happen.

For a signal with bandwidth B it is reasonable to regard any pair of terms in the RHS of (8) as resolved if they are separated by time-lags > $1/B$. Conversely, if the two terms are separated by less than, say, $1/2B$ they may be considered as overlapping. By (7) overlapping, and thereby cancellation, occurs when

$$r \geq \frac{d^2 B}{c} \qquad (9)$$

Considering sound propagating towards the receivers directly and via a bottom bounce is analogous to the surface reflection case apart from that the second and third term in the RHS of (8) change sign. Thus instead of cancellation at large distances we get constructive interference.

Finally a mixed case involving both surface and bottom reflections. An immediate implication for distances larger than d^2B/c, c.f. (7), is that the involved time-delays will be so small that surface contributions will interfere destructively, while the bottom contributions interfere constructively. At shorter distances there will be several resolved replicas of the emitted signal auto–correlation function, which will complicate the beam interpretation.

The second issue considered is the impact of the sound speed variation with depth upon the sound intensity at the receiver positions. The propagation model utilized is based on ray theory treating the sea bottom as perfectly absorbing. Furthermore the excitation frequency, being 200 Hz, is really below the applicability of the model. The spatial sound intensity variation shown in Figure 23 should therefore be considered as a rough approximation of the real sound propagation conditions. Still it constitutes an illustration of what could be the reason for the lower sound power levels registered by the left aperture of the hydrophone array. Crosses 1-3 and 3-5 mark tripodes pertaining to the left and right aperture respectively. It appears that the sound intensity between the two subaperture locations varies with at least 4 dB, which is consistent with what is seen on previously reported beam power plots.

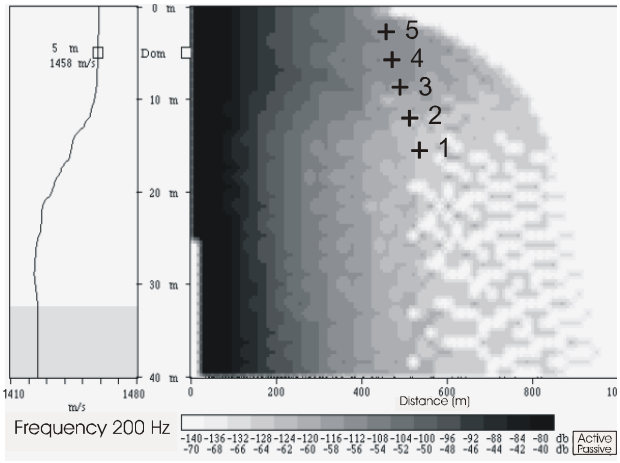

Figure 23. *Calculated sound intensity as a function of depth and range. Crosses mark the tripod hydrophone depths (see also figure 9). The source depth was 5 m. The sound speed profile utilized for the calculation was the blue curve in figure 10.*

The final issue considered is the impact of correlated noise, here thought of as shore reflections, at a sparsely populated array, constituted by the tripod hydrophones. Again a strongly simplified approach is utilized aiming to capture some of the behavior of this array in the stipulated environment. The shoreline is assumed to include some arcs strongly contributing as reflectors. One of these reflecting arcs was implemented by mirror sources at bearings 10° to 15°. Each mirror source emitted a replica of the excitation source at -20° but only with 20% of its power. Figure 24 shows the source wavelet as well as the mirror source contributions.

Notice that the central sensors of the array will sense the reflected sound field gained due to the directivity pattern of the 6 mirror sources. In addition to the strong peak pertaining to the source, the beam power plot in Figure 25 shows a second peak due to the shore reflection that is surpressed only by 0.6 dB.

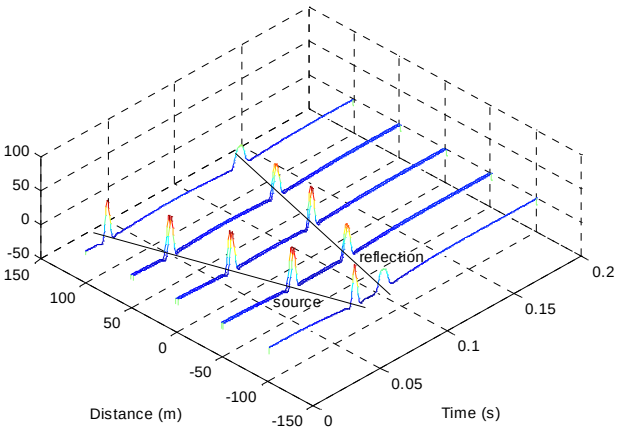

Figure 24. *The source wavelet plus mirror source contributions.*

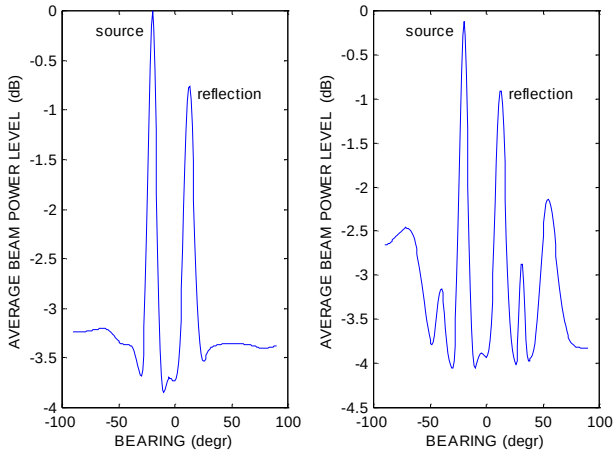

Figure 25. *FRAZ plot for the shore reflection simulation.*

5. Summary and conclusions

Simulations have demonstrated the implementation of a split-beam correlation algorithm. The split-beam processing technique was then applied on hydrophone array registrations of a stationary sound source in coastal shallow waters. The array processing requires the coherence lengths of the signal wave shapes to be of the same magnitude as the array aperture. A number of coherence measurements did therefore precede the split-beam processing experiment.

The coherence lengths, supported by the experimental site during the experiment, were estimated by analyzing narrowband-measurements. Coherence estimates for several frequencies were obtained using pairs of sensors with different sensor separation distances. In accordance with previous works on the subject, the coherence improved with decreasing integration time and bandwidth. Apart from some exceptions, coherence did also improve with decreased separation distances. The expected trend of coherence improvement with decreasing frequency was not evident. For the higher frequencies this behavior could be explained by changes in the speed of sound and wind (i.e. sea surface roughness), affecting the multipath propagation within the shallow water channel in a different way during each measurement. In the frequency band 0 – 250 Hz the experimental site most often supports coherence lengths of the order of 200 m.

Split-beam processing was carried out using signals from an approximately horizontal linear array sparsely populated with hydrophones. Signal distortion present in the recordings further reduced the number of sensors. The sensor spacing was then in the order of fifteen times larger than what is appropriate for the source signal bandwidth utilized. Grating lobes were introduced as a consequence, and the array gain became severely degraded. The coastal environment hosting the array, giving source signal reflections from the shore, further increased the destructive impact of the grating lobe presence. The beam power versus bearing plots did indicate the position of the sound source but they did also show a number of false bearing indications most likely due to the grating lobes. No statement based upon the ultimate perform-

ance of the split-beam correlation technique can therefore be made on the basis of the processed data. The particular choice of experimental site, array configuration as well as the choice of the rather weak sound source was imposed by the available equipment.

A future scope for the split-beam technique is to study its applicability in shallow waters. The horizontal arrays to be utilized should contain many wavelengths of the source signal components and still be populated by sensors separated by a moderate fraction of a half-wavelength. A rule of thumb has been derived here for accessing the multipath interference that may occur in such environments.

References

1 M. J. Beran, and G. B. Parrent, “Theory of partial coherence,” Prentice Hall, Canada, (1964).

2 V. H. Mac Donald and P. M. Shultheiss, “Optimum passive bearing estimation in a spatially incoherent noise environment,” J. Acoust. Soc. Am. 46, 37-43 (1969).

3 C. H. Knapp and G. C. Carter, “The generalized correlation method for estimation of time delay,” IEEE Trans. Acoust. Speech Signal Process. ASSP-24, 320-327 (1976).

4 S. Stergiopoulos and A. T. Ashley, “An experimental evaluation of split-beam processing as a broadband bearing estimator for line array sonar systems,” J. Acoust. Soc. Am. 102, 3556-3563 (1997).

5 V. Westerlin, “Koherens. Resultat från mätningar i Kalmarsund och i Stockholms skärgård,“ FOA rapport C 20878-2.2, Swedish Defence Research Est. (1992).

6 R. J. Urick, ”Principles of underwater sound,” 3rd edition, Peninsula Publishing, California (1983).

7 G. C. Carter, “Coherence and time delay estimation,” IEEE Proc. 75, NO 2 (1987).